Journal of Ovonic Research Vol. 14, No. 6, November - December 2018, p. 429 - 439

INFRARED REFLECTIVITY ANALYSIS OF Y^{3+} SUBSTITUTED $LaMnO_3$

J. AHMAD[a,*], H. ABBAS[a,b], S. H. BUKHARI[c], M. T. JAMIL[a], U. NISSAR[a], J. A. KHAN[a], S. A. ALI[a]
[a]*Department of Physics, Bahauddin Zakariya University, Multan 60800, Pakistan*
[b]*Department of Physics, Govt. Emerson College, Multan 60800, Pakistan*
[c]*Department of Physics, Govt. College University, Faisalabad, Layyah Campus, Layyah 31200, Pakistan*

Multiferroic manganite $La_{1-x}Y_xMnO_3$ (LYMO) (x=0.0, 0.2, 0.4, 0.6) have been synthesized by using sol-gel method. The powder X-ray diffraction (XRD) pattern with a Rietveld refinement analysis exhibits a transition from rhombohedral to orthrohombic for $0.4 \leq x \leq 0.6$. A comprehensive study of infrared (IR) active phonons was carried out at room temperature in the frequency range 30-7500 cm^{-1} by means of Fourier transform infrared (FTIR) spectrometer. Optical parameters i.e. resonant frequency ($\omega_{TO(j)}$), oscillator strength (S_j) and damping factor (Υ_j) of observed phonons have been determined by Lorentz oscillators model fit to the measured reflectivity. The frequency shifts of optical phonons have been observed with the increase in *x*. The change in optical parameters of IR active phonons reflects the confirmation of phase transformation. Moreover, Born and Szigeti effective charges were calculated to understand the polarization effect and ionicity in the present multiferroic system.

(Received May 31, 2018; Accepted November 19, 2018)

Keywords: X-ray diffraction, FTIR, infrared reflectivity, Energy band gap, Effective Charges

1. Introduction

The perovskite manganese oxides with general relation of $R_{1-x}A_xMnO_3$ (R =rare-earth and A=divalent element) have been widely investigated due to their colossal-magnetoresistance (CMR) effect near to the Curie temperature (T_C), which would be very important in many device applications [1]. The doped manganites provide the better physical properties by theoretical calculations in additional magnetic multiferroic phases [2-3]. For example, $La_{1-x}A_xMnO_3$ (A=Ca,Sr) have attracted interest much due to their huge negative magnetoresistance in range of doping concentration $0.2 \leq x \leq 0.5$ [4]. Different models are proposed to understand the origin of CMR in manganese oxides [5-7]. However, to a greater extent experimental and theoretical investigation predicts dynamic or static Jahn-Teller (JT) lattice distortion has a significant role in explanation of the CMR effects in the perovskite like manganese oxides [8-10]. Recently, the isotope shift in giant oxygen for the magnetoresistive perovskite $La_{1-x}Ca_xMnO_{3-\delta}$ observed and attributed this to a substantial JT effect and thus leads to a strong electron-phonon interaction which was the origin of JT polarons [11].

$La_{1-x}Ba_xMnO_3$ was the first reported CMR model composite with the Curie temperature of about 340 K [12]. The changes of crystal structure from orthorhombic to rhombohedral ($x > 0.13$) and to cubic ($x > 0.35$), in the system reveals ferromagnetic behavior for Ba concentrations $x \geq 0.15$ [13]. The mixed valence state (Mn^{3+}/Mn^{4+}) enhanced by a fractional substitution of the La^{3+} sites by the divalent alkaline earth ion and introduce the magnetic transition temperature in this system [14]. Such a transition has been explained for the double exchange (DE) interaction for Mn^{3+} and Mn^{4+} ions. It is advantageous to study the system by Mn-substitution, because such doping ions take place of Mn ions, therefore the precision of the Mn–O plane no longer exists, which will be an extensive change in structural and transport properties [14]. The perovskites of

*Corresponding author: dr.j.ahmad@gmail.com

$LaMnO_3$ exhibit an extraordinarily rich phase diagram due to different behavior of 3-d electrons, plotted with a function of magnetic field, temperature, and doping specifically due to the complex interchange of charge, spin, orbital, and lattice degree of freedom [15]. The synthesis conditions of the undoped parent compound $LaMnO_3$ show the different crystal structures [16-17]. For example, there are two well-determined phases that exist at room temperature: the orthorhombically distorted (space group *Pnma*) and a rhombohedrally distorted (space group *R-3c*) [17]. A. Urushibara et.al observed the structural phase transition in the $La_{1-x}Sr_xMnO_3$ for x=0.17 [18]. Similarly, M. Arao *et.al* [19] noted the insulating state in $LaMnO_3$ that altered into the metallic behavior at x=0.16 by increasing the content of x at room temperature. This would appear to recommend that the structural phase transition act as a prompt of the metal-insulator transition. Even though a comprehensive study have been discussed on the structure relationship for the divalent cation doped $R_{1-x}A_xMnO_3$ compounds, data on trivalent and monovalent cation doping are yet limited [20–22]. We have studied $La_{1-x}Y_xMnO_3$, Mn^{3+} may be converted to Mn^{4+} and hence correspond to the cations valency distribution [23]. The atoms substitution at specific sites may affect the vibrational properties of the host material through the bonding strength, the mass, and ionic radius [24]. Thus, the vibrational spectroscopy including both the Raman and infrared are very effective techniques for understanding the role of A and B-site substitution in the multiferroics. Furthermore, infrared spectroscopy (IR) is mostly useful for the systems, where lattice and electrons are strongly coupled to the electron and phonon interactions [24].

In this paper, we report the preparation of $La_{1-x}Y_xMnO_3$ series by sol gel method in the concentration of $0.0 \leq x \leq 0.6$. Results of XRD for structural investigation, spectroscopic analysis for atomic vibration and the phase transition by comparing through XRD and the optical properties.

2. Experimental

The polycrystalline $La_{1-x}Y_xMnO_3$, where (x=0.0, 0.2, 0.4 and 0.6.) were synthesized by using sol-gel technique. The chemical used were $La(NO_3)_3.6H_2O$, $Y(NO)_3.6H_2O$ and $Mn(NO_3)_2.4H_2O$ with the standard stoichiometry ratio. The powders were weighted in their equivalent weight and dissolved in 50 ml of distilled water. The citric acid used as the chelating agent with the citric acid and nitrate molar ratio of 1.5:1. By dissolving all the chemicals in distillated water and stirred through hot plate magnetic stirrer, until make the solution in homogenous state. After continuous stirring and heating at 70 °C, we obtain the viscous gel which was pre-heated at 120 °C for 1 hour to make it dried gel and was grounded manually into fine powder.

The obtained blackish dry powder was sintered at 900 °C for 8 hours in a box furnace (LHT 02/17). Grinding the precursor to make the pure form of powder then pressed into pellets by using hydraulic press at pressure of 30 KN. XRD pattern collected with the standard Cu-Kα radiation (λ=1.5406Å). The reflectivity measurements were taken by using FTIR spectrometer (BRUKER VERTEX 80V). The IR measurement observed by the combination of two detectors DLaTGs with two beam splitters of KBr and Mylar in near infrared range (14000- 4000) cm^{-1} and in the mid infrared range (4000 to 300) cm^{-1}, respectively.

3. Results and discussion

The XRD patterns of Y doped $LaMnO_3$ are shown in Fig 1. The Rietveld refinement, JANA2006 program was used to analyze the sample to confirm the single-phase compound with homogeneous distorted perovskite structure. The background was modeled by PANalytical of the kind and the peak shape was described by a pseudo-Voigt function. The actual data is shown by the crosses and the calculated curve is superimposed on them. The difference between the calculated and experimental XRD patterns are shown in bottom line. A good agreement exit between the observed and calculated data. For the concentration of x=0.0, 0.2 and 0.4 the observed pattern is fitted with rhombohedral structure in the space group *R-3c*. At the concentration of

x=0.2 and 0.4, the XRD pattern are single phase which means Y ions have been successfully replaced at position of La ions, however for x=0.6 some other peaks splits which reflects the presence of phase transition. At 48° the peak splits into two portions at x=0.6, which corresponds to the distortion in phase from rhombohedral to orthorhombic, such distortion also reported by N. Erdenee. *et. al.* for x= 0.2 and 0.4, in $LaCoO_3$ for the structural transformation from rhombohedral to cubic [25]. The change in the structure was confirmed by increase in the concentration of Y from rhombohedral to orthorhombic with space group of *Pnma* at x=0.6, such sort of phase transition also reported earlier in $La_{1-x}Sr_x\ MnO_{3+\delta}$ [26]. The XRD pattern for x=0.6 fits well with the diffraction pattern of a rhombohedral structure of $LaMnO_3$. A. Wold. *et.al*. firstly, confirm the rhombohedral structure at room temperature by systematic study, influencing on the firing atmosphere of the resulted unit cell of $LaMnO_3$ samples, when the percentage of Mn^{4+} greater than 20% [27]. Further phase distortions was investigated in the structure of $LaMnO_3$ as rhombohedral, orthorhombic or cubic depending on the concentration of Mn^{4+}, such as for 0–12%, 18–30%, the Mn^{4+} concentration and more than the 30%, $LaMnO_3$ becomes rhombohedral, orthorhombic and cubic, respectively [28]. Recently, Y.D. Zhao *et.al.* found that stoichiometric $LaMnO_3$ must be prepared in the lack of oxygen but sintering in ambient air consequences in nonstoichiometric $LaMnO_{3+\delta}$ with the arrangement of Mn^{4+}ions larger than 20% and by means of rhombohedral structure [29]. Accordingly, for our sample LYMO, sintered in the presence of oxygen, structure found rhombohedrally at room temperature, which indicate larger than 20% of Mn^{4+} ions. The grain size was calculated from expansion of XRD positions by Scherrer equation. Quantitatively, the position of peaks result can be used to improve the lattice constants for a certain unit cell. The atomic size of La and Y are 250pm and 240pm, by the increase in concentration of Y, its size may be predicted that cause the distortion in the structure occurs at x=0.6 which also confirmed by decrease in the grain size. The particle size for each sample is the diameter of individual grain and can be calculated from XRD pattern by using the standard Debye Scherrer formula [31].

$$D = k\,\lambda/\beta\cos\Theta \qquad (1)$$

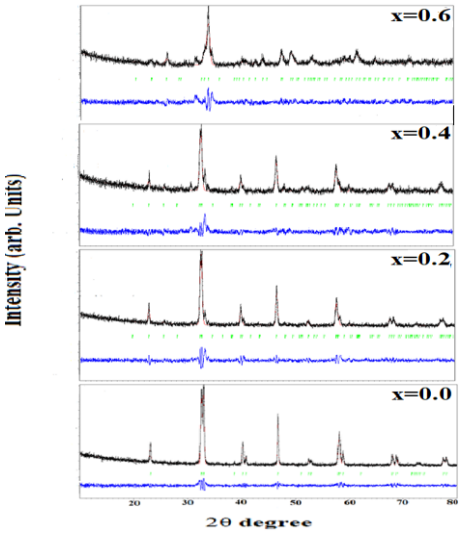

Fig. 1. Typical data of x-ray diffraction profiles for $La_{1-x}Y_x\ MnO_3$ (x=0.0, 0.2, 0.4, 0.6). Key: observed data (+) (black) and calculated profile (red), solid line, difference plots (blue) drawn below each profile, and tick marks (green) represent allowed Bragg reflections. The inset splitting of the main peak confirms the rhombohedral distortion of lattice also calculated by the doping of $LaMnO_3$ [30].

The variation of the lattice parameters *a* and *c* with x-concentration is shown in Fig. 2. There is the systematic decrease in the lattice parameters and the cell volume by increasing *x*, predicting the increase of Mn^{4+} content with x, which is quite similar to the previous observation [32, 33]**.** The presence of smaller cations in the B sublattice of the ABO_3 perovskite is responsible for the reduction in unit cell volume. The possible origins in the lattice distortion of perovskite based structures is the deformation of the Mn^{3+} O_6 octahedra originating from the J-T effect which is natural to the high-spin (S=2) Mn^{+3} ions for dual degeneracy of orbits. Evidently, such kind of distortion is related directly to the Mn^{+3} ions concentration [34].

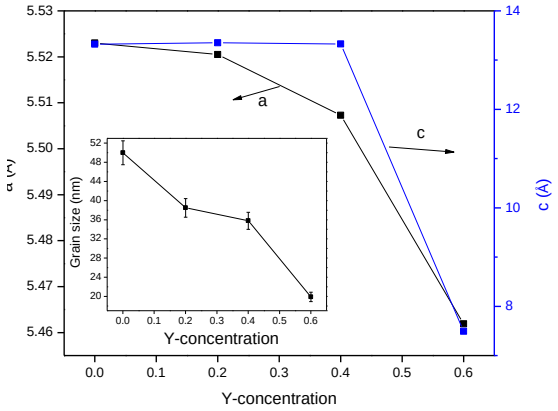

Fig. 2. The variation of the lattice parameters a and c with x, inset shows the change in the particle size for $La_{1-x}Y_x\ MnO_3$.

The IR spectra are shown in the range of 30-800 cm^{-1} at room temperature. However, the spectrum above 800 cm^{-1} is almost flat and structure-less, as shown in Fig.3, which means the absence of any electronic excitation at high frequency. Moreover, the infrared reflectivity (IR) spectra of polycrystalline LYMO are shown in Fig.4. In case of multiferroic materials, coupling of electric and magnetic orders can be investigated using infrared spectroscopy [35,36], with the help of Lorentz oscillator model. In this model, the total number of phonons must be equal to the total number of oscillators and then model is fitted to experimental reflectivity spectra using the relation

$$\varepsilon(\omega) = \varepsilon_{\infty} + \frac{\sum_j \omega_{TO}^2(j) S_j}{\omega_{TO(j)-\omega^2-i\omega\gamma_j}} \tag{2}$$

where, $\boldsymbol{\varepsilon}_{\infty}$ is the high frequency dielectric constant, $\boldsymbol{\omega}_{TO(j)}$ is the resonant frequency of transverse optical (TO) of jth phonon mode, Υ_j is the damping factor and S_j the oscillator strength of j^{th} optical phonon mode. To obtained the reflectivity at near normal incidence we use the Fresnal formula to correlate the dielectric function with the IR reflectivity, given as [37],

$$R(\omega) = \left|\frac{\sqrt{\epsilon(\omega)}-1}{\sqrt{\epsilon(\omega)}+1}\right|^2 \tag{3}$$

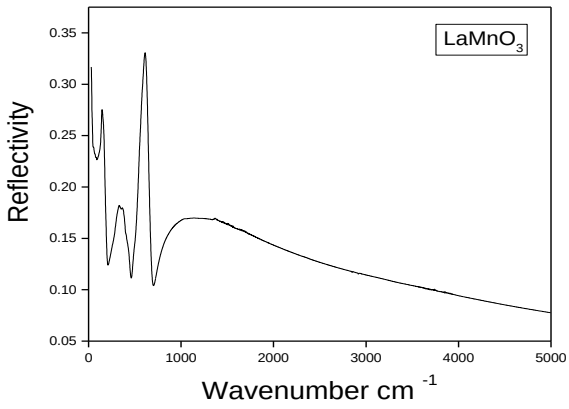

Fig. 3. Reflectivity spectrum of $LaMnO_3$.

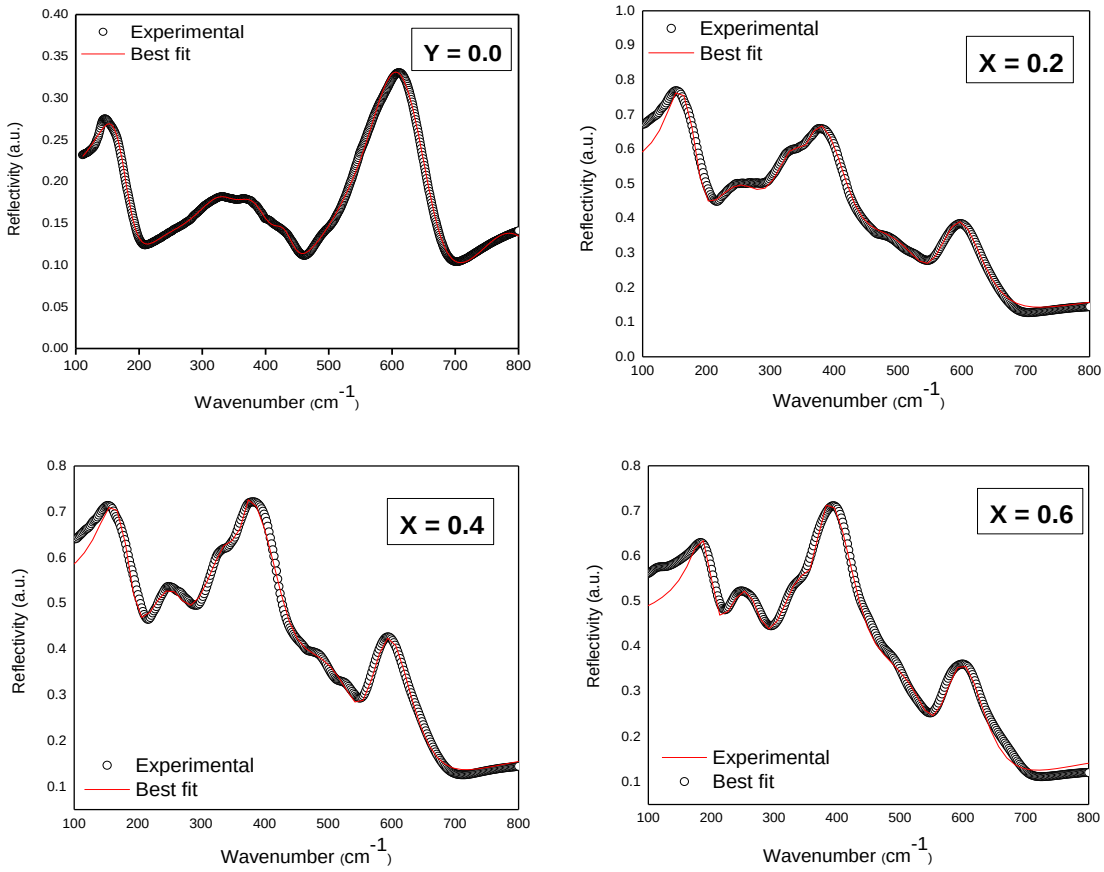

Fig. 4. IR Reflectivity spectra for $La_{1-x}Y_x\ MnO_3$.

The reflectivity spectra of LYMO for x= 0.0, 0.2, 0.4 and 0.6, show the numbers of reflection peaks attributed to (TO) phonons. The spectra rich in phonon modes are of a typical semiconductor nature and the sharp peaks correspond to the concentration dependence of ions displacement. The solid line represents the theoretical spectra obtained from the Lorentz oscillator fit to experimental reflectivity spectra, the fit parameters have been tabulated in Table 1. Four phonon modes observed in the IR spectrum of base sample $LaMnO_3$ and three new phonon modes are observed for x=0.2, 0.4 and 0.6. Basically, the bands of phonons can be classified into three modes, external phonons low frequency band (ω<290 cm^{-1}), the intermediate band as stretching band and the high frequency stretching band in the range (ω>590 cm^{-1}) [38]. To understand,

which atoms play the major role in LYMO, we investigate the frequencies of infrared active phonon (TO and LO). Most of the TO phonons observed in the intermediate band may appear due to the stretching band, corresponding to the phase distortion in LYMO as found by Taka-Hisa in $GdFeO_3$ type distortion [39].

Table 1. Phonon-fit parameters of the infrared reflectivity spectrum of LYMO $\omega_{TO(LO)}$ *in* cm^{-1} *the damping factor (**Y**), oscillator strength (**S**) and high frequency dielectric constant (*ε_∞*) are given below.*

X	**0.0**	**0.2**	**0.4**	**0.6**
ω_{TO1}	162	148.9	154.9	183.6
$\omega_{TO1}^{/}$	_	253.2	251.7	254.7
ω_{TO2}	336	330	334.9	340
ω_{TO3}	384	364.3	365.3	373.1
$\omega_{TO3}^{/}$	_	485	485	480
$\omega_{TO3}^{//}$	_	514.2	522	509.7
ω_{TO4}	588	596.8	597	600
ω_{LO1}	191	192.7	194.2	206.1
$\omega_{LO1}^{/}$	_	273.5	269.4	277.5
ω_{LO2}	341	341	351.5	350
$\omega_{LO3}^{/}$	403	445.6	437.6	449.6
$\omega_{LO3}^{//}$	700	768.3	536.9	531.6
ω_{LO4}	_		710.5	693
S_1	8.9	19.9	19.4	7.8
$S_1^{/}$	5.4	6.1	4.7	4.5
S_2	3.4	3.5	6.2	3
S_3	0.9	1.8	1.1	2.5
$S_3^{/}$	_	1.4	1.3	1.5
$S_3^{//}$	_	0.5	0.5	0.4
S_4	_	1.2	1.4	1
Y_1	57	26.1	37.2	30.4
$Y_1^{/}$	80	100	66.9	59.2
Y_2	72	47.9	60	51.4
Y_3	79	39.4	22.5	28.7
$Y_3^{/}$	_	165	175	176.2
$Y_3^{//}$	_	100	90	90
Y_4	_	72.8	65.1	70.6
ε_∞	**7.5**	**8.6**	**8.8**	**7.9**
ε_o	**26.0**	**43.0**	**24.1**	**28.5**

Interestingly, there are seven modes in doped LMO which is quite similar to the seven modes for $HoMnO_3$ and six modes for $LuMnO_3$ [40] which explain the superexchange between rare earth and manganese having important role in the multiferroic character of hexagonal manganites [41]. Interestingly, observed spectra of doped LYMO is much batter resolved than the base sample which is probably due to the distortion in the structure as confirmed by the Retrived refinement in the XRD pattern. In the external mode, new phonons $\omega_{TO1}^{/}$ at (x=0.2) 253.2, 251.7 and 254.7 cm^{-1}, which may be the relative motion of La-atoms with respect to MnO_6 octahedra, discussed earlier by K.H. Kim *et. al.* in $La_{0.5}Ca_{0.5}MnO_3$ [42]. In bending mode, two phonons $\omega_{TO3}^{/}$, $\omega_{TO3}^{//}$ appear at x=0.2, 0.4, 0.6, which correspond to the change in angle between Mn-O ions, known as JT distortion [43]. Interestingly, noted an additional weak mode detected around 500 cm^{-1} also reported by P. Calvani *et. al.* in the IR spectra of $LaAlO_3$ that were assigned to the cubic distortion due to the vibration of Al atoms from the zone boundary, so we can also expect as the phase distortion in LYMO due to the vibration of Y atoms in the whole compound [44, 45]. The increase in frequency occurs in ω_{TO4} from 588 to 600 cm^{-1} and no new phonon observed in the stretching mode, correspond to the internal motion of the Mn ions against octahedron of oxygen atoms or interestingly the bond length of Mn-O atoms [43]. G.D. Marzi *et.al* studied the phonons

in the rhombohedral structure having almost similar values in our work also reported in the lattice dynamics calculations of $LaMnO_3$ [46].

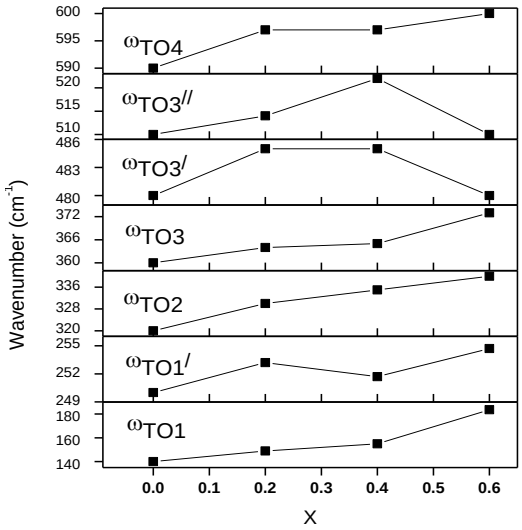

Fig.5. Concentration dependent of high frequency modes of LMO.

We have calculated the σ_1 (ω) spectra for the electronic structure of $La_{1-x}Y_xMnO_3$ investigated quantitatively, by using the relation [37],

$$\sigma_1(\omega) = \omega\varepsilon_2/4\pi \quad (4)$$

$\sigma_1(0)$ is zero imposing that at low frequency range there is no contribution from free carriers and also suggesting the localized charge carrier. Further, the band gap of optical energy has been counted from the optical conductivity spectra. From Fig.5, with the increase of *x*, decreases the band gap (E_g) and thus increases the conductivity of Y doped $LaMnO_3$, remarkably. The un-doped sample has insulating behavior which shifts toward the metallic behavior by increasing Y substitution. The value of E_g changes as *x* increases, which is insulating to metallic behavior, as shown in Fig.6. Interestingly, a phase change in $La_{1-x}Sr_xMnO_3$ was observed as the state of antiferromagnetic to ferromagnetic around x=0.1 and consequently the low-temperature ferromagnetic phase undergo an insulator-to-metal transition around x=0.17 [47-50].

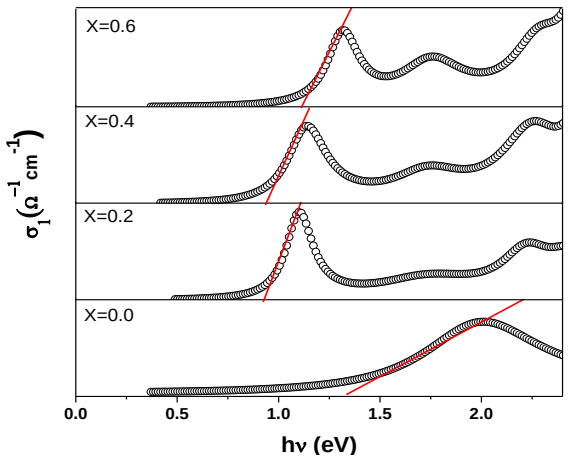

Fig. 6. The real part of optical conductivity (σ_1 (ω)) extracted from the reflectivity pattern.

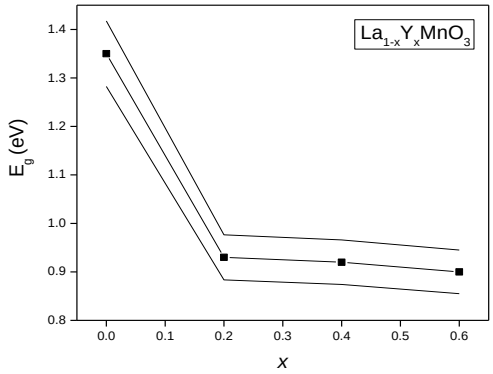

Fig. 7. Variation of the energy gap with the increase in concentration.

4. Born effective charge

By using the fitting reflectivity spectra with Drude-Lorentz oscillators, we have calculated $\overset{*}{Z}_k$ which also justify the macroscopic electric responses of a crystal to the interior dislocations of these atoms. These effective charges can be deliberate from phonon fit limitations meanwhile they are openly associated to effective transverse frequencies ω_{TO} [51], such that

$$\frac{4\pi}{v_c}\sum_{k=1}^{n}\frac{z_k^{*2}}{m_k} = 4\pi^2\sum_{j=1}^{N}(\omega_{LOj}^2 - \omega_{TOj}^2) \tag{5}$$

where, v_c represents the unit cell volume, j is the phonon mode, and m_k mass of atoms k. Note that Born effective charges include together static, ionic and dynamic electronic assistances to the dipole moment encouraged by electric field. In any oxides crystals, the Born Effective charges can be evaluated on the basis of longitudinal optical (LO) mode and transverse optical (TO) mode or through the phonon frequencies [52]. Born effective charges ($\overset{*}{Z}_k$) are also indication of interaction for Coulomb long range forces as compared with the short range forces, which leads to the transition in ferroelectrics [53]. For larger values of Born effective charges, it is generally considered to be reliable indications of the main tendency of an insulator leads for instability in ferroelectric.

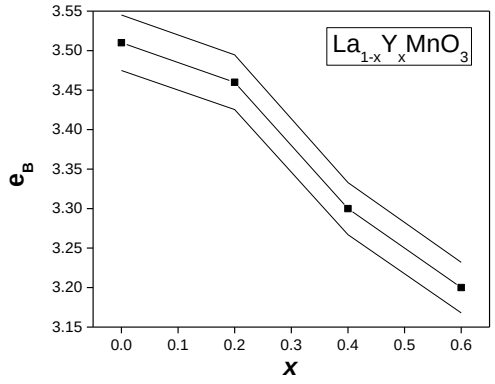

Fig. 8. Born effective charge of LYMO with the composition dependence.

The values for $La_{1-x}Y_xMnO_3$ are calculated using equation (4) for concentration x=0.0, 0.2, 0.4 and 0.6 are 3.51, 3.46, 3.30 and 3.2 respectively. With increasing the concentration, the values of ($\check{Z}_k$) decreases, which means the decrease in electric response.

5. The Szigeti effective charges

For the study of polarization effect and ionicity Szigeti (ionic) effective charges are intended from LO-TO splitting with the optical phonon modes. The extraordinary ionic system describing by ionic charges, while static and dynamic polarizations through the Born effective charges. Ions displacement in the system induced by the electron movement along the bond axis that is considered as the main source of Szigeti charges.

$$Z^*=\varepsilon_\infty^{1/2}Z^{(S)} \tag{6}$$

The values calculated from Eq. (6) for $La_{1-x}Y_xMnO_3$ (x=0.0, 0.2, 0.4 and 0.6) are 9.61, 6.5, 2.5 and 0.961. The variation in the values for Szigeti effective charges are shown in Fig. 9. It is clearly seen that the value of Szigeti charge does not remains same with increasing the substitution of Y-atoms, its value decrease like born effective charge.

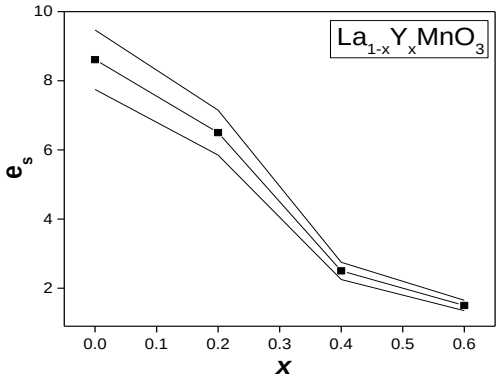

Fig. 9. The Szigeti effective charge with the composition dependence.

6. Conclusions

In conclusion, $La_{1-x}Y_x$ MnO_3 multiferroic materials have been synthesized by sol-gel technique for x=0.0, 0.2, 0.4, 0.6. The structural change in sample was analyzed using XRD technique, Rietveld refinement of the XRD has revealed that structural phase transition occur from rhombohedral to the orthorhombic. The average crystallite size is determined by Debye-Scherrer formula and found to be in 21 – 49 nm range. In all samples, the structural deviations from the ideal cubic perovskite structure might be resulted due to large number of phonons possibly originating from the tilting of MnO_6 octahedra or some coupling phenomena.

Moreover, the number of phonon modes are increased due to doping which is due to the appearance of new modes or the splitting of phonon modes. There is a decrease in the band gap with Y concentration, which depicts the insulator to metal transition. The Born and Szigeti effective charges decrease with increasing the concentration which consequently is an indication of shift of ionicity due to electric and magnetic polarization.

References

[1] Y. Tokura (ed.) Colossal Magneto-Resistive Oxides (New York: Gordon and Breach) (2000).
[2] G. Giovannetti, S. Kumar, J. van den Brink, S. Picozzi, Phys. Rev. Lett. **103**, 037601 (2009).
[3] S. Dong, R. Yu, J. M. Liu, E. Dagotto, Phys. Rev. Lett. **103**, 107204 (2009).
[4] G. H. Jonker, J. H. van Santen, Phys. (Utrecht) **16**, 337 (1950).
[5] Y. Tokura, A. Urushibara, Y. Moritomo, T. Arima, A. Asamitsu, J. Phys. Soc. **63**, 3931 (1994).
[6] R. M. Kusters, J. Singeton, D. A. Keen, R. McGreevy, W. Hay, Phys. B **155**, 362 (1989).
[7] J. Z. Liu, J. C. Chang, S. Inons, P. Klavins, R. N. Shelton, K. Song, S. R. Wasserman, Appl. Phys. Lett.**66**, 3218 (1995).
[8] A. J. Millis, P. R. Littlewood, B. I. Shraiman, Phys. Rev. Lett.**74**, 5144 (1995).
[9] A. J. Millis, Phys. Rev. B **53**, 8434 (1995).
[10] H. Roeder, J. Zang, A. R. Bishop, Phys. Rev. Lett. **76**, 1356 (1996).
[11] G. Zhao, K. Conder, H. Keller, K. A. Mueller, Natu. Lond. **381**, (1996).
[12] V. Helmolt, R. Wecker, J. Holzapfel, B. Schultz, L. Samwer, K. Phys. Rev. Lett. **71**, 2331 (1993).
[13] J. H. L. Nam, Y. S. Lee, J. E. Shin, H. S. J. Magn. Magn. Mater. **1**, 219 (2000).
[14] W. Khan, A. H. Naqvi, M. Gupta, S. Husain, R. Kumar, J. Chem. Phys. **135**, 054501 (2011).
[15] K. Kuepper, M. C. Falub, K. C. Prince, V. R. Galakhov, I. O. Troyanchuk, S. G. Chiuzbaian, M. Matteucci, X. D. Wett, O. R. Szargan, O. N. A. Ovechkina, Y. M. Mukovskii, M. Neumann, J. Phys. Chem. B, **109**, 9354 (2005).
[16] G. Zhao, K. Conder, H. Keller, K. A. Muller, Nat. Lon. **381**, 676 (1996).
[17] P. Norby, I. G. Krogh Andersen, E. K. Andersen, J. Sol. Sta. Chem. **119**, 191 (1995).
[18] A. Urushibara, Y. Moritomo, T. Arima, A. Asamitsu, G. Kido, Y. Tokura, Phys. Rev. B **51**, 103995).
[19] M. Arao, Y. Koyama, Phys. Rev. B **62**, 9 (2000).
[20] M. Itoh, T. Shimura, J. D. Yu, T. Hayashi, Y. Inaguma, Phys. Rev. B **522**, 5212 (1995).
[21] G. H. Rao, J. R. Sun, K. Barner, N. Hamad, J. Phys. Condens. Matt. **11**, 1523 (1999).
[22] C. Boudaya, L. Laroussi, E. Dhahri, J. C. Joubert, C. A. Rouhou, J. Phys. Condens. Matt. **10,** 748598).
[23] S. Roy, Y. Q. Guo, S. Venkatesh, N. Ali, J. Phys. Condens. Matt. **13**, 9547 (2001).
[24] G. D. Marzi, Z. V. Popovic, A. Cantarero, Z. D. Mitrovic, N. Paunovic, J. Bok, F. Sapin, Phys. Rev. B **68**, 064302 (2003).
[25] N. Erdenee, U. Enkhnaran, S. Galsan, A. Pagvajav, Hind. Jour. Nanomater. **8,** 9120586 (2017).
[26] J. F. Mitchell, D. N. Argyriou, C. D. Potter, D. G. Hinks, J. D. Jorgensen, S. D. Bader, Phys. Rev. B **54**, 9 (1996).
[27] A. Wold, R. Arnott, J. Phys. Chem. Sol. **9**, 176 (1959).
[28] A. Gholizadeh, J. Adv. Mater. Proc. **3**, 71 (2015).
[29] Y. D. Zhao, J. Park, R. J. Jung, H. J. Noh, S. J. Oh, J. Magn. Magn. Mater. **280**, 404 (2004).
[30] D. Varshneya, N. Dodiya, J. Mater. Res. **29**, 1183 (2014).
[31] A. L. Patterson, Phys. Rev. **56** (1939).
[32] Z. Serpil, J. Gopalakrishnan, S. A. Sirchio, B. W. Eichhorn, V. Smolyaninova, R. L. Greene J. Sol. Sta. Chem. **159**, 68 (2001).
[33] I. D. Fawcett, E. Kim, M. Greenblatt, Phys. Rev. B, **62** (2000).
[34] D. Varshneya, N. Dodiya, J. Mater. Res. **29**, 1183 (2014).
[35] R. P. S. N. Lobo, R. L. Moreia, D. D. Lebeugle, D. Colson, Phys. Rev. B, **76**, 172105 (2007).
[36] M. Zaghrioui, V. T. Phuoc, R. A. Souza, M. Gervais, Phys. Rev. B **78**, 184305 (2008).
[37] J. Ahmad, S. H. Bukhari, M. T. Jamil, M. K. Rehmani, H. Ahmad, T. Sultan, Hind. Adv. Cond. Matt. Phys, **8**, 5389573 (2017).
[38] J. Kim, S. Jung, M. S. Park, S. I. Lee, H. D. Drew, H. Cheong, K. H. Kim, E. J. Choi, Phys. Rev. B, **74**, 052406 (2006).
[39] T. Hisa, Y. Tokura, J. Phys. Soci. Jap., **l64**, 2488 (1995).
[40] J. Vermette, S. Jandl,Phys. Rev. B **85**, 134445 (2012).

[41] J. Vermette, S. Jandl, A. A. Mukhin, V. Y. Ivanov, A. Balbashov, M. M. Gospodinov, L. P. Gaudart, J. Phys. Condens. Matt. **22**, 356002 (2010).
[42] K. H. Kim, J. Y. Gu, H. S. Choi, G. W. Park, T. W. Noh, P hys. Rev. Lett. **26** (1996).
[43] Z. V. Popovic, A. Cantarero, Z. D. Mitrovic, N. Paunovic, J. Bok, F. Sapi, Phys. Rev. **68**, 064302 (2003).
[44] P. Calvani, M. Capizzi, F. Donato, P. Dore, S. Lupi, P. Maselli, C. P. Varsamis, Phys. C **181**, (1991).
[45] Z. M. Zhang, B. I. Choi, M. I. Fink, A. C. Anderson, J. Opt. Soc. Am. B **11**, 2252 (1994).
[46] G. D. Marzi, M. V. Abrashev, A. P. Litvinchuk, M.N. Iliev, R. L. Meng, V. N. Popov, V. G. Ivanov, R. A. Chakalov, C. Thomsen, Phys. Rev. B **59**, 4146 (1999).
[47] G. H. Jonker, J. H. van Santen, Phys. **16**, 337 (1950).
[48] E. O. Wollan, W. C. Coehler, Phys. Rev. **100**, 545 (1955).
[49] Y. Tokura, A. Urushibara, Y. Moritomo, A. Asamitsu, G. Kido, N. Furukawa, J. Phys. Soc. **63**, 418 (1994).
[50] M. Paraskevopoulos, F. Mayr, C. Hartinger, A. Pimenov, J. Hemberger, P. Lunkenheimer, A. Loidl, A.A. Mukhin, V.Y. Ivanov, A.M. Balbashov, J. Magn. Magn. Mat. **211**, 118 (2000).
[51] S. Jandl, S. Mansouri, M. Orlita, J. Phys. Conds. Matt. **25**, 475403 (2013).
[52] F. Gervais, Sol. Stat. Comm. **18**, 191 (1976).
[53] P. Ghosez, X. Gonze, P. Lambin, J. P. Michenaud, Phys. Rev. B, **51**, 6765 (1995).